analytical chemistry

pubs.acs.org/ac Article

Drug-to-Antibody Ratio Estimation via Proteoform Peak Integration in the Analysis of Antibody−Oligonucleotide Conjugates with Orbitrap Fourier Transform Mass Spectrometry

Konstantin O. Nagornov, Natalia Gasilova, Anton N. Kozhinov, Pasi Virta, Patrik Holm, Laure Menin, Victor J. Nesatyy, and Yury O. Tsybin*

Cite This: *Anal. Chem.* 2021, 93, 12930−12937 Read Online

ACCESS | Metrics & More | Article Recommendations | Supporting Information

ABSTRACT: The therapeutic efficacy and pharmacokinetics of antibody−drug conjugates (ADCs) in general, and antibody−oligonucleotide conjugates (AOCs) in particular, depend on the drug-to-antibody ratio (DAR) distribution and average value. The DAR is considered a critical quality attribute, and information pertaining to it needs to be gathered during ADC/AOC development, production, and storage. However, because of the high structural complexity of ADC/AOC samples, particularly in the initial drug-development stages, the application of the current state-of-the-art mass spectrometric approaches can be limited for DAR analysis. Here, we demonstrate a novel approach for the analysis of complex ADC/AOC samples, following native size-exclusion chromatography Orbitrap Fourier transform mass spectrometry (FTMS). The approach is based on the integration of the proteoform-level mass spectral peaks in order to provide an estimate of the DAR distribution and its average value with less than 10% error. The peak integration is performed via a truncation of the Orbitrap's unreduced time-domain ion signals (transients) before mass spectra generation via FT processing. Transient recording and processing are undertaken using an external data acquisition system, FTMS Booster X2, coupled to a Q Exactive HF Orbitrap FTMS instrument. This approach has been applied to the analysis of whole and subunit-level trastuzumab conjugates with oligonucleotides. The obtained results indicate that ADC/AOC sample purification or simplification procedures, for example, deglycosylation, could be omitted or minimized prior to the DAR analysis, streamlining the drug-development process.

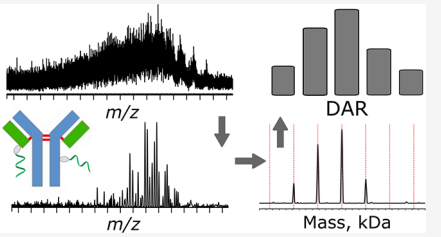

INTRODUCTION

Antibody−drug conjugates (ADCs) are immunoconjugates that combine the capabilities of monoclonal antibodies (mAbs) to reach cancer cells and the antitumor properties of cytotoxic drugs to induce chemotherapy action within cancer cells.[1−6] The conjugation reaction between drug molecules and a mAb typically yields a heterogeneous mixture of ADCs, characterized by a range of drug-to-antibody ratio (DAR) values.[5,7] This range is subsequently used to calculate the average DAR value, a critical quality attribute of ADCs that denote the average number of cytotoxic molecules per mAb molecule. The rapidly progressing ADC discovery and development processes require efficient and high-throughput analytical methods enabling accurate and reliable ADC characterization, including DAR analysis.[5,8−10] A particular example of complex ADC samples is the antibody−oligonucleotide conjugates (AOCs).[11,12] Compared to the traditional small molecule-based ADCs, the AOCs may be more difficult to analyze because of an increased payload size and the notorious effects on the optimal ionization conditions of the payload.[13]

High levels of selectivity and specificity of mass spectrometry (MS), typically coupled to liquid chromatography (LC), render it an analytical technique of choice to provide the required accuracy needed in deducing the DAR values.[2,9,14,15] The currently employed MS methods differ by the resolution performance (low vs high resolution) and the degree of protein unfolding (denaturing vs native MS conditions).[1,4,16−18] The native MS approach has been shown to have advantages for the analysis of both noncovalently and covalently bound ADC samples compared to analysis performed under denaturing conditions.[1,4,16,17] Lower-resolution levels, ∼5000−15,000 at the target m/z peak, are common for mass measurements of proteins in the native MS approach.[16,17,19−21] Analysis of ADCs/AOCs of a low-to-medium sample complexity could be efficiently conducted with Orbitrap Fourier transform MS (FTMS),[8,9,20−23] time-of-flight (TOF) MS,[4,18,20,24] and triple quadrupole MS platforms.[25] The increased complexity of ADC samples has paved the way to a broader application of high-resolution MS instruments,[22,26] which may still prove to be

Received: May 28, 2021
Revised: August 31, 2021
Accepted: September 1, 2021
Published: September 14, 2021

Downloaded via UNIV OF TURKU on November 1, 2021 at 09:04:45 (UTC).
See https://pubs.acs.org/sharingguidelines for options on how to legitimately share published articles.

ACS Publications

© 2021 The Authors. Published by American Chemical Society

https://doi.org/10.1021/acs.analchem.1c02247
Anal. Chem. 2021, 93, 12930−12937

inadequate at resolving highly congested mass spectra derived from complex ADC/AOC samples.

To facilitate intact mass measurements, the number of ADC/AOC proteoforms, which represents individual unmodified or modified species,[27] can be reduced both in solution (e.g., by deglycosylation)[12,28] and in vacuo (e.g., by ion mobility).[29] Another sample simplification routine is the decomposition of intact mAbs into subunits, such as heavy and light chains (*Hc* and *Lc*, respectively), $F(ab)_2$, $F(ab)$, *Fd′*, *Fc*, and *Fc*/2 subunits.[23,30,31] Mass analysis of these subunits is known as a middle-up MS approach.[23,30,32] Practical implementation of native MS approaches involves liquid separation with techniques that do not cause protein denaturation in the aqueous mobile phase, such as size-exclusion chromatography (SEC).[33] The usual SEC run is about 5−7 min, which is often faster than the typical high-performance liquid chromatography (HPLC) separation employed in denaturing MS.[9] As a result, the native SEC−MS combination has gained particular attention for the DAR analysis.[15,18] It can compare equally or favorably to various LC methods, which are typically employed for DAR analysis, with or without MS as a detector.[15,18,34]

Despite significant progress in the methods described above, the sheer magnitude of the number of multiple ADC/AOC proteoforms present in highly complex ADC/AOC samples may prevent the estimation of DARs even by high-resolution native SEC−MS. Both the LC elution profile and the mass spectra of intact proteins may be represented as unresolvable congestion of chromatographic and spectral features that cannot be adequately analyzed, for example, via deconvolution, to deliver the appropriate accuracy of an average DAR estimate. One of the approaches to tackle congested mass spectra is to apply the Fourier-domain harmonics to mass spectra of the polydisperse ion populations with repeated subunits.[35,36] Similarly, the deconvolution of the highly polydisperse mass spectral data from the ADC-like species has been rationalized with the comb filter approach.[20] An alternative approach to declutter such patterns, an individual ion-counting MS, recognizes and leverages the space-charge influence on peak interference, resulting in congested mass spectra.[37,38] The potentially valuable applications of these methods for the (whole, complex) ADC/AOC analysis are yet to be validated. In addition, the sample handling procedures, such as purification, deglycosylation, and enzymatic digestion, may introduce artifacts and increase sample preparation time.[18] Therefore, the development of easy-to-implement FTMS approaches, potentially relaxing sample preparation needs, is welcome to address the complex ADC/AOC sample analysis challenge.

It is well known that the integration of mass spectral peaks belonging to different isotopologues of an individual protein present in a given charge state improves the signal-to-noise ratio (SNR) of the lower-resolution peaks.[19,39−44] This leads to the advantage of performing average, instead of the isotopically resolved, mass analysis of heavier than 30 kDa proteins.[40] Here, we extend this approach and demonstrate that integrating mass spectral peaks that belong to different ADC/AOC proteoforms may resolve congested mass spectra of complex samples and facilitate rapid estimation of DAR distributions and average DAR values. The determined optimum degree of proteoform integration may require resolution performance lower than that accessible commercially to a general Orbitrap FTMS user. To address this deficiency, we employed an external high-performance data acquisition (DAQ) system that enabled acquisition and postprocessing of the unreduced time-domain FTMS data, known as transients.

METHODS

Trastuzumab-Oligonucleotide Conjugation. First, trastuzumab, an antibody of isotype IgG1, was treated with NHS-PEG4-azide (Figure S1) to yield the antibody-cross-linker conjugate. Upon attachment to a Lys side chain, this bifunctional cross-linker adds a $C_{11}H_{19}N_3O_5$ moiety (monoisotopic mass 273.13247 Da and an average mass 273.29 Da) to the mAb. Second, a dibenzocyclooctyne (DBCO)-triethylene glycol-modified oligonucleotide was assembled using commercially available conventional phosphoramidite building blocks (see Appendix S1). The quality control analysis of the employed oligonucleotide confirmed its purity and returned its average molecular weight of about 6977.8 Da (Figure S2). Finally, the antibody cross-linker conjugate and the DBCO-oligonucleotide were mixed to yield a ∼ 7.2 kDa mAb modification (Figure S3).

Sample Preparation for Middle-Up Analysis. The trastuzumab cross-linker conjugate was digested with IdeS and then submitted to disulfide bond reduction with tris(2-carboxyethyl)phosphine to yield 25 kDa subunits, namely, *Lc*, *Fc*/2, and *Fd′*. In parallel, the AOC sample was digested with IdeS without disulfide bond reduction, yielding ∼100 kDa $F(ab')_2$ and its complementary ∼50 kDa *Fc* subunit (or two ∼25 kDa *Fc*/2 subunits). For more details, see Appendix S1.

Liquid Chromatography−Mass Spectrometry. Sample separation by HPLC was performed using an analytical HPLC system (Ultimate 3000, Thermo Fisher Scientific, Bremen, Germany) with 30 min run duration and an analytical column Acquity BEH (ethylene bridged hybrid) technology C4 (1.7 μm, 300 Å, 1 × 150 mm, Waters AG, Baden-Dättwil, Switzerland) at 90 μL/min and 60 °C. The SEC separation was carried out on the same analytical HPLC system with a 7 min run duration using a conventional SEC column (MAbPac SEC-1, 5 μm, 300 Å, 4 × 150 mm; Thermo Fisher Scientific). The following amounts of samples were used per experiment: middle-up HPLC−FTMS: 0.2−0.5 μg; SEC−FTMS: 10−20 μg.

A Q Exactive HF Orbitrap FTMS instrument (Thermo Fisher Scientific) equipped with the BioPharma option was employed to acquire all experimental data. IdeS-digested trastuzumab cross-linker conjugate samples were analyzed using HPLC-Orbitrap FTMS under denaturing conditions. Intact and IdeS-digested AOC samples were analyzed with the SEC−Orbitrap FTMS under native conditions. Mass spectra were acquired in positive-ion mode using electrospray ionization (ESI). The following settings were employed: HPLC−FTMS: AGC = 3e6, maximum injection time IT_{max} = 500 ms, R = 240,000 at 200 m/z (transient length, T_{acq} = 512 ms), in-source CID of 20 eV; SEC−FTMS: AGC = 5e6, auto IT_{max}, R = 60,000 at 200 m/z (T_{acq} = 128 ms), and in-source CID of 75−150 eV. The *.RAW reduced profile mass spectra were obtained in enhanced FT or eFT mode.

Time-Domain Transient Acquisition from Orbitrap FTMS. The Orbitrap FTMS was operated via a standard in-built DAQ station and instrument control software (Xcalibur, Thermo Fisher Scientific). In parallel, it was coupled to an external high-performance DAQ system (FTMS Booster X2, Spectroswiss, Lausanne, Switzerland). Previously, similar

https://doi.org/10.1021/acs.analchem.1c02247
Anal. Chem. 2021, 93, 12930−12937

external DAQ systems were interfaced with Q Exactive Orbitrap FTMS instruments for small molecule analyses.[45,46] The lengths of the transients acquired with the external and the in-built DAQ systems were comparable.

FTMS Data Processing and Analysis. The time-domain transients recorded with the FTMS Booster X2 were apodized with half-window Kaiser-type function, zero-filled twice, and converted into absorption-mode Fourier transform (aFT) mass spectra using Peak-by-Peak software (version 2021.4.1, Spectroswiss). Procedures of transient truncation and lower-resolution aFT mass spectra generation were performed using the same software. The mass spectra were baseline-corrected using a model-free method that estimates the baseline using the median of the noise extrema.[47] Baseline correction parameters were adjusted for each transient duration. The baseline-corrected mass spectra were noise-thresholded at the level of six standard deviations of noise and peak picked.

High-resolution middle-up protein data were deisotoped and deconvolved using the Hardklör algorithm,[48] integrated into Peak-by-Peak. The low-resolution data were deconvolved and interpreted using the UniDec deconvolution software.[49] Batches of deconvolved mass spectra were automatically analyzed using the in-house-written Peak-by-Peak software tool to calculate DARs. The DAR calculations were performed based on the mass spectra peak intensities I_n (after deconvolution) using the following standard formula:[15]

$$\mathrm{DAR} = \frac{\sum_{n=0}^{m} (I_n \times n)}{\sum_{n=0}^{m} I_n}$$

where n is the DAR number, and m is the maximum DAR number for a given sample.

RESULTS AND DISCUSSION

A Proteoform Integration Workflow. By analogy with the isotopologue peak integration of the isotopic envelopes belonging to the individual proteoforms, we propose integrating mass spectral peaks originating from several proteoforms of ADCs/AOCs. In addition to the glycosylation and payload conjugation, these proteoforms may arise from the ADC/AOC complexation with impurities, reagents, and reaction intermediate species generated during ADC/AOC production. The proteoform integration workflow formulated here has been designed specifically for FTMS (Figure 1).

A particular requirement for an efficient implementation of the proteoform integration workflow is the generation of mass spectra with a reduced resolution. Moreover, the ADC/AOC sample complexity may require generating mass spectra at a resolution level below the lowest resolution provided by a given commercial FTMS instrument. That can be achieved by (i) generating lower-resolution mass spectra on-the-fly or (ii) via user-controlled truncation of the acquired time-domain transients, followed by Fourier transform (even the shortest time-domain transients delivered by the FTMS instruments may be too long to provide the required lower-resolution levels). The manufacturers typically restrict both options. However, owing to the recent advances in data acquisition electronics and allied digital signal processing, the time-domain data can be obtained from the contemporary FTMS instruments using the external high-performance DAQ systems and provided for data processing.[45,46,50]

In practice, the optimum resolution (transient duration) for the analysis of a particular ADC/AOC sample may be unknown a priori. It was the case in the current work, where the limited sample amount (<100 μg) and expectedly high sample complexity suggested using a (relatively) high-resolution setting on an Orbitrap FTMS (60,000 at m/z 200, which requires 128 ms transients) (Figure 1). As a result, the initially attempted high-resolution intact mass measurements of the AOC samples have revealed particularly complex and convolved proteoform peak distributions for both the intermediates and the final AOC product (see below).

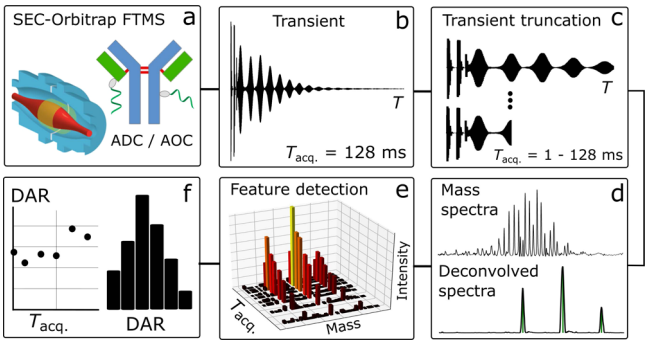

Figure 1. Proteoform integration workflow for DAR estimation using Orbitrap FTMS: (a) typical ADC/AOC sample analysis starts with sample separation using SEC, followed by ionization and mass measurements conducted under native MS conditions; (b) time-domain transients of a user-defined length are acquired (transient period of 128 ms is given as an example); (c) data postprocessing starts with in silico transient truncation; (d) ADC/AOC mass spectra and deconvolved mass spectra are generated for the full and truncated transients with a baseline correction;[47] (e) manual or automatic DAR feature detection based on the combined analysis of all deconvolved mass spectra; and (f) optimum transient length for a given ADC sample is determined, and final DAR metrics are extracted: DAR distribution and an average DAR value.

Orbitrap FTMS Analysis of Trastuzumab Conjugated with Cross-Linkers. The intact mass measurements of trastuzumab with cross-linkers were performed using native-mode SEC−Orbitrap FTMS (Figure S4). The mass spectra produced by spectral or transient averaging over a complete elution profile between 3.8 and 4.8 min are depicted in Figure S5. The initially selected resolution setting of 60,000 at m/z 200 (128 ms transients, Figure S5a) resulted in a complex mass spectrum exhibiting two unresolvable patterns in the mass range of 5000−6500 m/z (Figure S5b). The deconvolved mass spectrum shows many peaks in the mass range of ∼150 kDa (Figure S5c). However, the deconvolution results could not be easily rationalized and employed to estimate the number of cross-linkers attached to trastuzumab. A closer look into the time-domain transients shows a prominent first isotopic beat in the initial period of ion detection, followed by a long analyte signal-free stretch (Figure S5a). To reduce the mass spectral complexity and increase SNR values for the proteoforms, the same 128 ms transients were in silico-truncated to 32 ms and processed in absorption-mode FT (aFT) to generate lower-resolution mass spectra. Notably, a transient duration of 32 ms corresponds to the lowest resolution setting (15,000 at m/z 200) for the employed Orbitrap instrument (Figure S5d). Nevertheless, the corresponding mass spectrum (Figure S5e) and its deconvolved counterpart (Figure S5f) still challenge peak annotation.

Serendipitously, by further truncating the transient, we realized that shorter transients provide a step-change in data quality. For example, as short as 6 ms transients (Figure S5g),

https://doi.org/10.1021/acs.analchem.1c02247
Anal. Chem. 2021, 93, 12930−12937

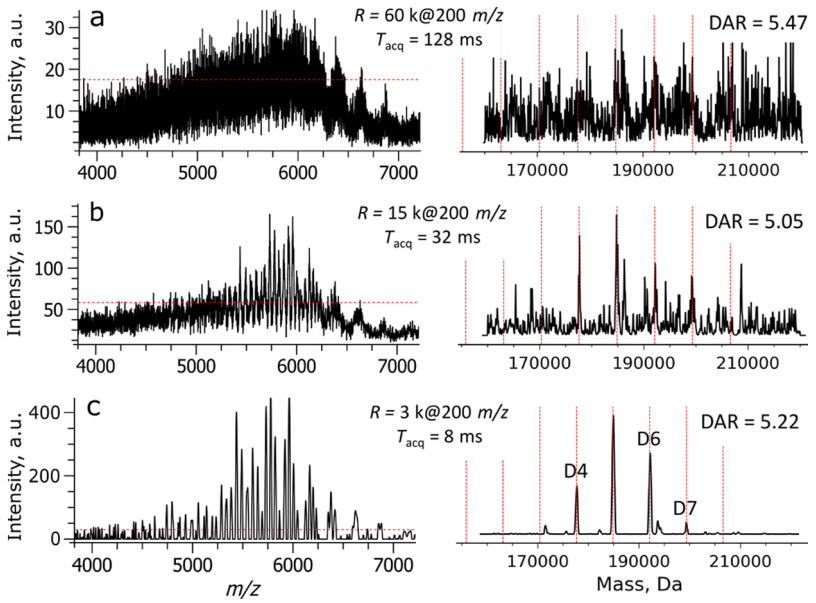

Figure 2. Revealing proteoforms of an intact AOC sample using SEC−Orbitrap FTMS analysis. The left column shows mass spectra produced via a standard workflow (spectral averaging) at the diverse transient lengths of (a) 128 ms, eFT and (b) 32 ms, aFT; and via a proteoform integration workflow (transient averaging, baseline correction) at (c) 8 ms, aFT. The right column shows the results of a deconvolution procedure of the corresponding mass spectra revealing the DAR distributions for the target peaks (red vertical lines). The noise thresholding levels are indicated with the horizontal red lines. Averaging of scan data has been performed over a complete elution profile.

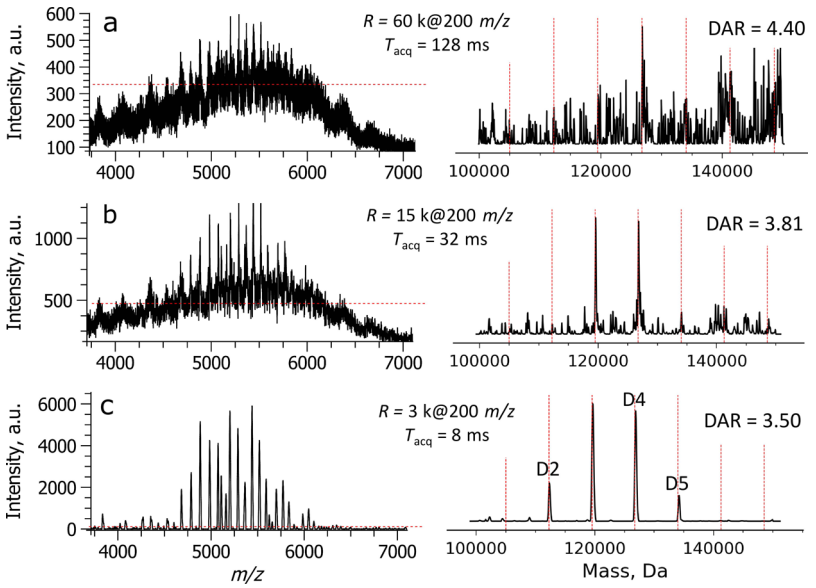

Figure 3. Revealing proteoforms of an $F(ab')_2$ subunit of the AOC sample using SEC−Orbitrap FTMS analysis. The left column shows mass spectra produced via a standard workflow (spectral averaging) at the diverse transient lengths of (a) 128 ms, eFT and (b) 32 ms, aFT; and via a proteoform integration workflow (transient averaging, baseline correction) at (c) 8 ms, aFT. Right column shows the results of a deconvolution procedure of the corresponding mass spectra revealing the DAR distributions for the target peaks (red vertical lines). The noise thresholding levels are indicated with the horizontal red lines. Averaging of scan data has been performed over a complete elution profile.

yield mass spectra that exhibit the two peak distributions that could be annotated as peaks corresponding to the unmodified and modified with cross-linker species (Figure S5h). The intensities of the observed peaks in the mass spectra obtained from the 6 ms transients (Figure S5h) are more than 10-fold and 50-fold higher compared to the results of 32 ms (Figure S5e) and 128 ms (Figure S5b) transient processing, respectively. The subsequent deconvolution of the low-resolution mass spectrum (Figure S5h) resulted in the two strong signals with about 2 kDa mass difference. The observed mass change and peak width suggest that about seven-to-eight cross-linkers are conjugated, on average, to an intact trastuzumab (a mass shift of 273.29 Da is gained upon single cross-linker addition, Figure S1).

To confirm the abovementioned estimate of the number of the attached cross-linkers, we performed a middle-up analysis of the same modified trastuzumab (Figures S6−S10). Briefly, the *Fc*/2 subunits, which correspond to the C-terminal part of the heavy chain, exhibited the expected glycosylation pattern as well as the presence of at least one cross-linker per subunit

https://doi.org/10.1021/acs.analchem.1c02247
Anal. Chem. 2021, 93, 12930−12937

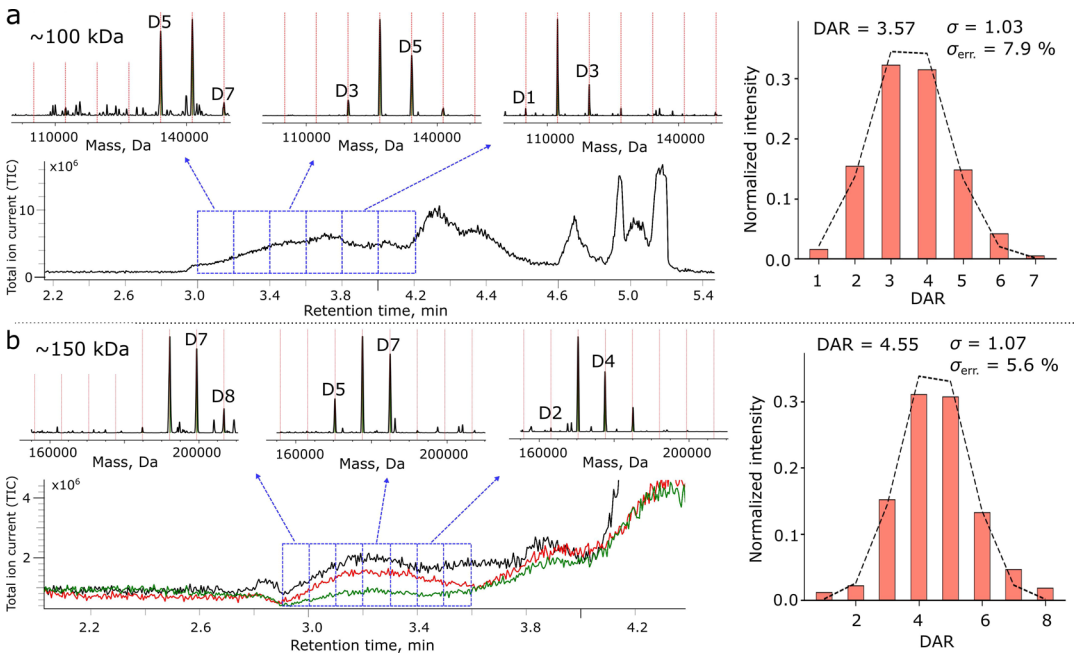

Figure 4. AOC sample analysis with SEC−Orbitrap FTMS utilizing short, 8 ms, transients. DAR values of (a) ~100 kDa $F(ab')_2$ subunit of the AOC sample and (b) ~150 kDa intact AOC sample obtained as results of data processing with a sliding window of 0.2 min for the $F(ab')_2$ subunit and 0.1 min for intact AOC along the elution profile: initial section, middle section, and prelast section. The right column shows the total DAR distributions produced by averaging the results of the sliding window approach for the target peaks (red vertical lines).

(Figure S8). The Lc subunits exhibited up to three cross-linkers per subunit (Figure S9). Finally, analysis of the Fd′ subunit, which corresponds to the N-terminal part of the heavy chain, showed the presence of up to four cross-linkers (Figure S10). Therefore, the middle-up analysis of trastuzumab subunits suggests up to eight cross-linkers distributed among all subunits, with their preferential conjugation within the N-terminal mAb part above the hinge region.

Orbitrap FTMS Analysis of Trastuzumab Conjugated with Oligonucleotides. The final AOC sample, trastuzumab conjugated with the heavy, 7 kDa, oligonucleotide drugs, presents a structurally more complicated sample compared to the trastuzumab modified with cross-linkers. As expected, its initial high-resolution Orbitrap FTMS intact mass measurements yielded a highly convolved proteoform peak pattern (Figure 2). The results reported in Figure 2 correspond to the data integration over a complete elution profile from about 2.9−3.6 min, as shown in Figure S11.

The original setting of 60,000 at m/z 200 produced an elevation of spectral features in a mass spectrum that could not be efficiently deconvolved (Figure 2a). Reducing the resolution to the lowest possible setting on the employed instrument, 15,000 at m/z 200, via postprocessing, resulted in a visually less-complex set of peaks (Figure 2b). The deconvolution output produced several peaks that may be attributed to the AOC species but are buried in the matrix of other similar-intensity peaks. Interestingly, a further fourfold reduction in resolution revealed a clear distribution of AOC peaks to which DAR distribution can be assigned straightforwardly (Figure 2c). The optimum transient length of ~8 ms employed to generate these results is comparable to the one found suitable for the analysis of the intermediate AOC species in the current work (Figure S5) and in an earlier report on 30−60 kDa protein analysis by Fornelli and co-workers.[40]

Orbitrap FTMS Analysis of an $F(ab')_2$ Subunit of the AOC Sample. In an attempt to estimate DAR distribution directly with the accessible Orbitrap FTMS resolution settings, we reduced the structural complexity of the AOC sample described in Figure 2 by performing the IdeS digestion of trastuzumab below the hinge region. As expected, it resulted in a generation of a 100 kDa N-terminal $F(ab')_2$ subunit (Figure 3). The presented results correspond to the data integrated over a complete elution profile, between about 3 and 4.2 min, as shown in Figure S12.

Modifying the AOC sample by enzymatically removing a 50 kDa C-terminal *Fc* subunit, which carries most glycosylations, represents a significant reduction in sample complexity. Nevertheless, the final truncated AOC sample is still too complex for a high-resolution MS analysis (Figure 3a). Reduction in resolution to 15,000 at m/z 200 produced a visibly less-convolved mass spectrum, which starts to show the drug-to-subunit (DSR) distribution (Figure 3b). Meanwhile, the deconvolved mass spectrum remains noisy and exhibits many artifactual peaks. Finally, transient truncation to the same length of 8 ms, as employed previously, yields a distinct DSR distribution (Figure 3c). The distance between the (truncated) AOC peaks can now be measured to be ~7250 Da, which corresponds to the molecular weight of an individual oligonucleotide drug.

DAR Estimation. The low-resolution mass measurements performed on both the intact AOC sample and its drug-conjugated $F(ab')_2$ subunit revealed distinct payload distributions (Figures 2c and 3c). As discussed above, these distributions were obtained for data integration over complete elution periods. The intact 150 kDa AOC analysis suggested that the most prominent number of drugs conjugated to trastuzumab is 5, followed by 6, 4, and 7 payloads (Figure 2c). The 100 kDa $F(ab')_2$ subunit analysis indicated that trastuzumab conjugation with 3 or 4 drugs is the most

https://doi.org/10.1021/acs.analchem.1c02247
Anal. Chem. 2021, 93, 12930−12937

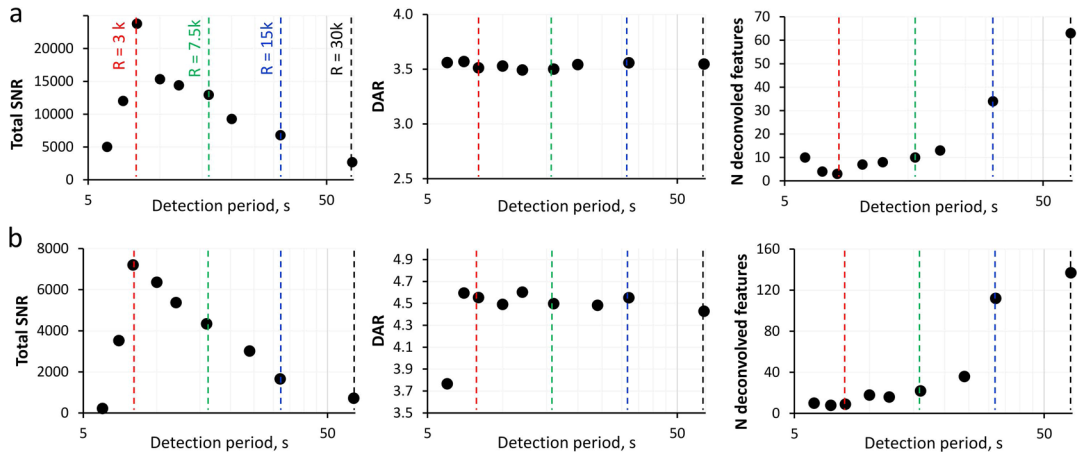

Figure 5. Evolution of DAR characteristics (total ion signal SNR, averaged DAR values, and the number of deconvolved features) as a function of the detection period. Results are shown for the (a) ~100 kDa $F(ab')_2$ subunit of AOC and (b) ~150 kDa intact AOC sample. These results were obtained using transient averaging (sliding window approach) and detection-period-dependent baseline correction of the experimental SEC−Orbitrap FTMS data.

prominent reaction outcome, followed by 2 and 5 payloads (Figure 3c). As a result, the average DAR/DSR is reduced from 5.22 for intact AOC to 3.50 for the $F(ab')_2$ subunit. It may be rationalized by the preferential, but not exclusive (Figures S8−S10), cross-linker location above the hinge region reported above.

On the other hand, it is an upcoming practice in LC−MS analysis of modified proteins in general and ADC/AOC samples, in particular, to perform data analysis gradually along the elution profile using a sliding window approach.[51] The application of this approach in the current analysis of trastuzumab conjugated with the cross-linkers is shown in Figure S13, and the AOC analysis is shown in Figure 4. The selection of the sliding window size shown in Figure 4 is directed by the elution time, 0.8 min, for the intact sample analysis (Figure S11) and 1.2 min for the (more abundant) subunit sample analysis (Figure S12). The evolution of the DSR distribution for the $F(ab')_2$ subunit shows that the species with a higher number of drugs conjugated to the trastuzumab elute earlier, as expected for SEC separation (Figure 4a). In contrast with the DSR distribution data presented in Figure 3c, the attachment of as many as six and seven drugs becomes visible. Furthermore, conjugation of fewer drugs, namely, two, becomes very prominent at the end of the elution period. As a result, averaging the DSR distributions obtained for the individual sliding window results in the average DSR value of 3.57 for the $F(ab')_2$ subunit of the AOC sample. The thus-obtained average DSR value is close to the 3.50 value obtained without the sliding window approach (Figure 3).

Similar behavior is observed for DAR estimation via the sliding window approach for the intact AOC (Figure 4b). The high payload species elute first, including AOCs with up to eight drugs conjugated. As low as DAR = 3 species become prominent at the end of the elution period. The resulting average DAR value is 4.55, with DAR = 4 and DAR = 5 as the most prominent channels. Notably, DAR = 3 and DAR = 8 channels are not visible in the DAR distribution obtained with data integration over the whole elution period (Figure 2c). As a result, the thus-obtained average DAR value is lower than the 5.22 value obtained without the sliding window approach (Figure 2). Both values can be considered as critical quality attributes awaiting further validation of the sliding window method. In addition, a standard deviation (σ) and its standard deviation error (σ_{err}) can be employed to describe DAR distributions (Figure 4).

Time-Dependent Feature Detection and DAR Estimation Approach. To select an appropriate resolution level producing sufficiently accurate DAR estimation for a given ADC/AOC sample, a gradual truncation of the experimentally acquired (long, *e.g.*, 64−128 ms) transient is to be performed in silico. The following characteristics could be monitored as a function of the detection period for a set of selected peaks (features), for example, those that describe the ADC/AOC species: the total SNR level, the average DAR value, and the total number of deconvolved features. Results of time-dependent DAR/DSR analysis performed for the user-estimated selected (target) peaks in the intact AOC and its $F(ab')_2$ subunit sample analysis are presented in Figure 5.

As expected from the transient isotopic beat pattern characteristic for mAb analysis,[52] increasing the transient length leads to a significant reduction in the total SNR level for whole AOC and its subunit cases. On the other hand, the number of deconvolved features increases with the increase in resolution. At the same time, reduction in the detection period drives proteoform integration and yields fewer features. The lower number and a higher SNR of the detected (integrated) features simplify data interpretation and reduce potential deconvolution artifacts. It translates into the average DAR dependence on the detection period for a set of target peaks. These characteristics show that the average DAR values from the shorter considered periods differ by less than 10% from the anticipated average DAR value across all the considered detection periods. The anticipated (true) average DAR value can be estimated from the (congested) higher resolution data once the target DAR peaks to monitor are revealed by the easy-to-follow lower-resolution mass spectra. Nevertheless, too short, <8 ms, transients may result in a drop in all monitored parameters. Therefore, the optimum transient length is sample-complexity-dependent.

The manual data analysis procedure, including feature (target ADC/AOC peaks) detection, applied to generate results in Figure 5 may be automated to optimize the selection of the optimum transient period (Figure S14). The automated data processing approach may offer more time points

https://doi.org/10.1021/acs.analchem.1c02247
Anal. Chem. 2021, 93, 12930−12937

(transient periods) describing the data quality attributes, speed up the entire data analysis routine, and exclude possible human factor-related analysis issues.

CONCLUSIONS

DAR analysis of complex ADC/AOC samples by contemporary native SEC−Orbitrap FTMS approaches has been shown to have method limitations because of the congestion of both SEC and FTMS features. This congestion has prevented the consequent mass spectral processing and eventual DAR characterization. To address this challenge, we proposed and developed an FTMS-centric proteoform integration approach. In order to benchmark this approach, we applied it to analyze an in-house-synthesized trastuzumab-oligonucleotide conjugate (AOC).

The reported experimental results demonstrate that a significant reduction in mass spectral resolution, below the commonly accessible and employed Orbitrap resolution levels, may lead to a straightforward and rapid estimation of DAR distributions and their average values. Resolution levels attainable with ∼8 ms time-domain transients may be taken as the initial approximation. Further optimization of the transient periods can be performed manually or automatically, as presented here. The final error of the described approach is shown to be within 10% of the anticipated average DAR value. Therefore, applying the proteoform peak integration processing has been demonstrated to be a viable and attractive approach specifically for the ADC/AOC analysis using Orbitrap FTMS instruments. The ability to perform both (very) high-resolution and the here-reported (very) low-resolution mass measurements on the same instrument further add to the Orbitrap's flexibility and versatility. Notably, the optimum resolution of the method deduced here can be lower than the minimum resolution levels provided by some other mass analyzers, e.g., TOF MS.

The practical implementation of the proteoform integration approach on Orbitrap FTMS platforms can be realized in multiple ways. First, some modern Orbitrap FTMS instruments may directly provide mass spectra with the resolution setting reduced to 7500 at m/z 200 (16 ms transients).[9] Second, users can be granted access to the time-domain transients from Orbitraps either by the instrument manufacturer (via the built-in DAQ systems), as employed previously,[53,54] or by utilizing external DAQ systems, for example, FTMS Booster X2, as employed in the current work. Availability of the time-domain transients adds flexibility and empowering capabilities to the postacquisition data processing.

Application-wise, the described approach may find utility for a rapid DAR estimation throughout the ADC/AOC development process, and it may potentially diminish the need for extensive sample purification prior to the MS analysis. By decreasing the need for extensive sample preparation prior to analysis, the potential for artifacts to be introduced would be reduced, thereby increasing the overall speed of the ADC/AOC development and subsequently reducing the overall cost. Overall, the experimental results suggest the method's potential wide applicability for a range of complex ADC/AOC samples, including those expected from novel classes of biotherapeutics, such as bispecific ADCs.

FINANCIAL CONFLICT OF INTEREST

Dr. Tsybin, Dr. Nagornov, and Dr. Kozhinov are employees of Spectroswiss, which develops hardware and software tools for FTMS data acquisition and processing.

ASSOCIATED CONTENT

Supporting Information

The Supporting Information is available free of charge at https://pubs.acs.org/doi/10.1021/acs.analchem.1c02247.

Experimental and method details. Schematic descriptions, assembly, and characterization data of the AOCs and its constituents. Results of SEC−Orbitrap FTMS analysis of an intact mAb (trastuzumab) modified with cross-linkers and of an intact AOC sample and its $F(ab')_2$ subunit. Results of a sliding window analysis of SEC−Orbitrap FTMS data. Middle-up analysis of trastuzumab modified with cross-linkers after IdeS digestion. A workflow for the automated definition of an optimum transient period (feature detection). (PDF)

AUTHOR INFORMATION

Corresponding Author

Yury O. Tsybin − *Spectroswiss, 1015 Lausanne, Switzerland;* orcid.org/0000-0001-7533-0774; Email: tsybin@spectroswiss.ch

Authors

Konstantin O. Nagornov − *Spectroswiss, 1015 Lausanne, Switzerland*

Natalia Gasilova − *Ecole Polytechnique Fédérale de Lausanne, 1015 Lausanne, Switzerland*

Anton N. Kozhinov − *Spectroswiss, 1015 Lausanne, Switzerland*

Pasi Virta − *Department of Chemistry, University of Turku, 20014 Turku, Finland;* orcid.org/0000-0002-6218-2212

Patrik Holm − *Protein and Antibody Engineering Unit, Orion Pharma, 20380 Turku, Finland*

Laure Menin − *Ecole Polytechnique Fédérale de Lausanne, 1015 Lausanne, Switzerland*

Victor J. Nesatyy − *Protein and Antibody Engineering Unit, Orion Pharma, 20380 Turku, Finland*

Complete contact information is available at: https://pubs.acs.org/10.1021/acs.analchem.1c02247

Notes

The authors declare the following competing financial interest(s): Dr. Tsybin, Dr. Nagornov, and Dr. Kozhinov are employees of Spectroswiss, which develops hardware and software tools for FTMS data acquisition and processing.

ACKNOWLEDGMENTS

We are grateful for the financial support through Spectroswiss Sàrl, Business Finland (448/31/2018), and the European Horizon 2020 research and innovation program under grant agreement #829157 (TopSpec).

REFERENCES

(1) Debaene, F.; Bœuf, A.; Wagner-Rousset, E.; Colas, O.; Ayoub, D.; Corvaïa, N.; Van Dorsselaer, A.; Beck, A.; Cianférani, S. *Anal. Chem.* **2014**, *86*, 10674−10683.

(2) Beck, A.; Terral, G.; Debaene, F.; Wagner-Rousset, E.; Marcoux, J.; Janin-Bussat, M.-C.; Colas, O.; Dorsselaer, A. V.; Cianférani, S. *Expert Rev. Proteomics* **2016**, *13*, 157−183.
(3) Beck, A.; Goetsch, L.; Dumontet, C.; Corvaïa, N. *Nat. Rev. Drug Discovery* **2017**, *16*, 315−337.
(4) Botzanowski, T.; Erb, S.; Hernandez-Alba, O.; Ehkirch, A.; Colas, O.; Wagner-Rousset, E.; Rabuka, D.; Beck, A.; Drake, P. M.; Cianférani, S. *mAbs* **2017**, *9*, 801−811.
(5) Joubert, N.; Beck, A.; Dumontet, C.; Denevault-Sabourin, C. *Pharmaceuticals* **2020**, *13*, 245.
(6) Birrer, M. J.; Moore, K. N.; Betella, I.; Bates, R. C. *J. Natl. Cancer Inst.* **2019**, *111*, 538−549.
(7) Xu, K.; Liu, L.; Dere, R.; Mai, E.; Erickson, R.; Hendricks, A.; Lin, K.; Junutula, J. R.; Kaur, S. *Bioanalysis* **2013**, *5*, 1057−1071.
(8) Zhu, X.; Huo, S.; Xue, C.; An, B.; Qu, J. *J. Pharm. Anal.* **2020**, *10*, 209−220.
(9) Huang, Y.; Mou, S.; Wang, Y.; Mu, R.; Liang, M.; Rosenbaum, A. I. *Anal. Chem.* **2021**, *93*, 6135−6144.
(10) Todoroki, K.; Mizuno, H.; Sugiyama, E.; Toyo'oka, T. *J. Pharm. Biomed.* **2020**, *179*, No. 112991.
(11) Dovgan, I.; Koniev, O.; Kolodych, S.; Wagner, A. *Bioconjug.* **2019**, *30*, 2483−2501.
(12) Dovgan, I.; Ehkirch, A.; Lehot, V.; Kuhn, I.; Koniev, O.; Kolodych, S.; Hentz, A.; Ripoll, M.; Ursuegui, S.; Nothisen, M.; et al. *Sci. Rep.* **2020**, *10*, 7691.
(13) Dugal-Tessier, J.; Thirumalairajan, S.; Jain, N. *J. Clin. Med.* **2021**, *10*, 838.
(14) Wakankar, A.; Chen, Y.; Gokarn, Y.; Jacobson, F. S. *mAbs* **2011**, *3*, 161−172.
(15) Jones, J.; Pack, L.; Hunter, J. H.; Valliere-Douglass, J. F. *mAbs* **2020**, *12*, No. 1682895.
(16) Rosati, S.; Rose, R. J.; Thompson, N. J.; van Duijn, E.; Damoc, E.; Denisov, E.; Makarov, A.; Heck, A. J. *Angew. Chem., Int. Ed. Engl.* **2012**, *51*, 12992−12996.
(17) Campuzano, I. D. G.; Sandoval, W. *J. Am. Soc. Mass Spectrom.* **2021**, 1861.
(18) Matsuda, Y.; Robles, V.; Malinao, M.-C.; Song, J.; Mendelsohn, B. A. *Anal. Chem.* **2019**, *91*, 12724−12732.
(19) Lössl, P.; Snijder, J.; Heck, A. J. R. *J. Am. Soc. Mass Spectrom.* **2014**, *25*, 906−917.
(20) Campuzano, I. D. G.; Robinson, J. H.; Hui, J. O.; Shi, S. D. H.; Netirojjanakul, C.; Nshanian, M.; Egea, P. F.; Lippens, J. L.; Bagal, D.; Loo, J. A.; et al. *Anal. Chem.* **2019**, *91*, 9472−9480.
(21) Campuzano, I. D. G.; Nshanian, M.; Spahr, C.; Lantz, C.; Netirojjanakul, C.; Li, H.; Wongkongkathep, P.; Wolff, J. J.; Loo, J. A. *J. Am. Soc. Mass Spectrom.* **2020**, *31*, 1155−1162.
(22) He, J.; Kaur, S.; Xu, K. In *Antibody-Drug Conjugates: Methods and Protocols*, Tumey, L. N., Ed.; Springer US: New York, NY, 2020, pp. 213−219.
(23) Srzentić, K.; Fornelli, L.; Tsybin, Y. O.; Loo, J. A.; Seckler, H.; Agar, J. N.; Anderson, L. C.; Bai, D. L.; Beck, A.; Brodbelt, J. S.; et al. *J. Am. Soc. Mass Spectrom.* **2020**, *31*, 1783−1802.
(24) Källsten, M.; Hartmann, R.; Artemenko, K.; Lind, S. B.; Lehmann, F.; Bergquist, J. *Analyst* **2018**, *143*, 5487−5496.
(25) Källsten, M.; Pijnappel, M.; Hartmann, R.; Lehmann, F.; Kovac, L.; Lind, S. B.; Bergquist, J. *Anal. Bioanal. Chem.* **2019**, *411*, 2569−2576.
(26) He, J.; Su, D.; Ng, C.; Liu, L.; Yu, S.-F.; Pillow, T. H.; Del Rosario, G.; Darwish, M.; Lee, B.-C.; Ohri, R.; et al. *Anal. Chem.* **2017**, *89*, 5476−5483.
(27) Smith, L. M.; Kelleher, N. L.; The Consortium for Top Down Proteomics. *Nat. Methods* **2013**, *10*, 186.
(28) Wohlschlager, T.; Scheffler, K.; Forstenlehner, I. C.; Skala, W.; Senn, S.; Damoc, E.; Holzmann, J.; Huber, C. G. *Nat. Commun.* **2018**, *9*, 1713.
(29) Huang, R. Y. C.; Deyanova, E. G.; Passmore, D.; Rangan, V.; Deshpande, S.; Tymiak, A. A.; Chen, G. *J. Am. Soc. Mass Spectrom.* **2015**, *26*, 1791−1794.
(30) Faid, V.; Leblanc, Y.; Bihoreau, N.; Chevreux, G. *J. Pharm. Biomed.* **2018**, *149*, 541−546.
(31) Sjögren, J.; Andersson, L.; Mejàre, M.; Olsson, F. In Bacterial Pathogenesis: Methods and Protocols, Nordenfelt, P.; Collin, M., Eds.; Springer New York: New York, NY, 2017, pp. 319−329.
(32) Lermyte, F.; Tsybin, Y. O.; O'Connor, P. B.; Loo, J. A. *J. Am. Soc. Mass Spectrom.* **2019**, 1149.
(33) Liu, H.; Gaza-Bulseco, G.; Chumsae, C. *J. Am. Soc. Mass Spectrom.* **2009**, *20*, 2258−2264.
(34) Bobály, B.; Fleury-Souverain, S.; Beck, A.; Veuthey, J.-L.; Guillarme, D.; Fekete, S. *J. Pharm. Biomed.* **2018**, *147*, 493−505.
(35) Cleary, S. P.; Prell, J. S. *Analyst* **2020**, *145*, 4688−4697.
(36) Cleary, S. P.; Li, H.; Bagal, D.; Loo, J. A.; Campuzano, I. D. G.; Prell, J. S. *J. Am. Soc. Mass Spectrom.* **2018**, *29*, 2067−2080.
(37) Kafader, J. O.; Melani, R. D.; Durbin, K. R.; Ikwuagwu, B.; Early, B. P.; Fellers, R. T.; Beu, S. C.; Zabrouskov, V.; Makarov, A. A.; Maze, J. T.; et al. *Nat. Methods* **2020**, *17*, 391−394.
(38) Elliott, A. G.; Harper, C. C.; Lin, H.-W.; Williams, E. R. *Analyst* **2017**, *142*, 2760−2769.
(39) Nagornov, K. O.; Kozhinov, A. N.; Gasilova, N.; Menin, L.; Tsybin, Y. O. *J. Am. Soc. Mass Spectrom.* **2020**, *31*, 1927−1942.
(40) Fornelli, L.; Durbin, K. R.; Fellers, R. T.; Early, B. P.; Greer, J. B.; LeDuc, R. D.; Compton, P. D.; Kelleher, N. L. *J. Proteome Res.* **2017**, *16*, 609−618.
(41) Makarov, A.; Denisov, E. *J. Am. Soc. Mass Spectrom.* **2009**, *20*, 1486−1495.
(42) Compton, P. D.; Zamdborg, L.; Thomas, P. M.; Kelleher, N. L. *Anal. Chem.* **2011**, *83*, 6868−6874.
(43) Kafader, J. O.; Melani, R. D.; Schachner, L. F.; Ives, A. N.; Patrie, S. M.; Kelleher, N. L.; Compton, P. D. *J. Am. Soc. Mass Spectrom.* **2020**, *31*, 574−581.
(44) Marshall, A. G.; Hendrickson, C. L.; Shi, S. D. H. *Anal. Chem.* **2002**, *74*, 252 A−259 A.
(45) Nagornov, K. O.; Zennegg, M.; Kozhinov, A. N.; Tsybin, Y. O.; Bleiner, D. *J. Am. Soc. Mass Spectrom.* **2020**, *31*, 257−266.
(46) Bills, J. R.; Nagornov, K. O.; Kozhinov, A. N.; Williams, T. J.; Tsybin, Y. O.; Marcus, R. K. *J. Am. Soc. Mass Spectrom.* **2021**, 1224.
(47) Friedrichs, M. S. *J. Biomol. NMR* **1995**, *5*, 147−153.
(48) Hoopmann, M. R.; Finney, G. L.; MacCoss, M. J. *Anal. Chem.* **2007**, *79*, 5620−5632.
(49) Marty, M. T.; Baldwin, A. J.; Marklund, E. G.; Hochberg, G. K. A.; Benesch, J. L. P.; Robinson, C. V. *Anal. Chem.* **2015**, *87*, 4370−4376.
(50) Kooijman, P. C.; Nagornov, K. O.; Kozhinov, A. N.; Kilgour, D. P. A.; Tsybin, Y. O.; Heeren, R. M. A.; Ellis, S. R. *Sci. Rep.* **2019**, *9*, 8.
(51) Millán-Martín, S.; Carillo, S.; Füssl, F.; Sutton, J.; Gazis, P.; Cook, K.; Scheffler, K.; Bones, J. *Eur. J. Pharm. Biopharm.* **2021**, *158*, 83−95.
(52) Denisov, E.; Damoc, E.; Makarov, A. Exploring Frontiers of Orbitrap Performance for Long Transients. *Int. J. Mass Spectrom.* **2021**, *116607*.
(53) Fornelli, L.; Damoc, E.; Thomas, P. M.; Kelleher, N. L.; Aizikov, K.; Denisov, E.; Makarov, A.; Tsybin, Y. O. *Mol. Cell. Proteomics* **2012**, *11*, 1758−1767.
(54) Srzentić, K.; Nagornov, K. O.; Fornelli, L.; Lobas, A. A.; Ayoub, D.; Kozhinov, A. N.; Gasilova, N.; Menin, L.; Beck, A.; Gorshkov, M. V.; et al. *Anal. Chem.* **2018**, *90*, 12527−12535.

https://doi.org/10.1021/acs.analchem.1c02247
Anal. Chem. 2021, 93, 12930−12937